

Hiroyuki Yamamoto · Kentaro Abe · Yoshiharu Arakawa
Takashi Okuyama · Joseph Gril

Role of the gelatinous layer (G-layer) on the origin of the physical properties of the tension wood of *Acer sieboldianum*

Received: September 17, 2003 / Accepted: April 12, 2004

Abstract The tension wood (TW) properties of a 70-year-old specimen of *Acer sieboldianum* Miq. were analyzed by using the G-fiber model that was proposed in our previous report. The roles of the G-layer on the origins of (1) a high tensile growth stress, (2) a large longitudinal Young's modulus, and (3) a high longitudinal drying shrinkage in the TW xylem are discussed on the basis of the simulations using the G-fiber model. The results suggest that the G-layer generates a high tensile stress in the longitudinal direction during xylem maturation; the longitudinal Young's modulus of the green G-layer becomes significantly higher than that of the lignified layer; furthermore, the G-layer tends to shrink extraordinarily more than that of the lignified layer during moisture desorption.

Key words Cellulose microfibril · Gelatinous fiber · Growth stress · Wood cell wall · Reaction wood

Introduction

Tension wood (TW) shows abnormal xylem properties when compared with the normal wood (NW), e.g., large tensile growth stress, high longitudinal Young's modulus, and large longitudinal shrinkage after drying. Some researchers attribute such behaviors to the physical properties

of the gelatinous layer (G-layer) through comparing xylem properties and anatomical features in the TW xylem.^{1–4}

To verify these ideas, it is required to observe the behaviors or physical properties of the G-layer by isolating it directly from the lignified layer. However, it is almost impossible to obtain the G-layer cylinder without inflicting any damage. No matter how a G-layer cylinder is isolated, it is still difficult to provide an accurate measurement because the G-layer cylinder is too small to be analyzed by a conventional mechanical testing machine.

The authors consider that simulation using a mathematical model of the multilayered wood fiber gives one of the most effective approaches for estimating the behavior of each cell wall constituent as it exists in the cell wall.⁵ In our previous report, we proposed a structural model of the G-fiber consisting of four-layered cylinders (CML + S1 + S2 + G), and formulated the mechanical behaviors of the G-fiber model on the basis of the reinforced-matrix hypothesis.⁶

The formula derived in the previous report contains several parameters. We need to optimize those parameters to obtain a reasonable result when we simulate the observed phenomena on the basis of the G-fiber model. Conversely, it can be considered that the optimized values of the parameters should reflect certain internal properties and fine composite structures of each constituent material in the G-layer. In this report, based on the simulation using the G-fiber model, we analyze the observed results for the physical properties of the TW xylem from an inclined stem of a 70-year-old kohauchiwakaede (*Acer sieboldianum* Miq.), and we explain the role of the G-layer on the origin of distinctive xylem properties in the TW.

H. Yamamoto (✉) · K. Abe · Y. Arakawa · T. Okuyama
School of Bioagricultural Sciences, Nagoya University, Chikusa,
Nagoya 464-8601, Japan
Tel. +81-52-789-4152; Fax +81-52-789-4150
e-mail: hiro@agr.nagoya-u.ac.jp

J. Gril
Laboratoire de Mécanique et Génie Civil, Université Montpellier 2,
34095 Montpellier, France

This report follows the previous report "Role of the gelatinous layer on the origin of the physical properties of the tension wood." J Wood Sci (2004) 50:197–208. Part of this paper was presented at the 49th Annual Meeting of the Japan Wood Research Society, Tokyo, April 1999, and at the 2nd International Conference of the European Society for Wood Mechanics, Stockholm, May 2003

Experiment

Material and method

A 70-year-old kohauchiwakaede (*Acer sieboldianum* Miq.), grown on the steep slope of a private mountain in Kiyomi-

Table 1. Observed data for a 70-year-old kohauchiwakaede (*Acer sieboldianum* Miq.)

Measuring positions	1	2	3	4	5	6	7	8	9	10
Area composition of domain of each tissue (%) measured at low magnification										
Vessel [<i>V</i>]	7.2	6.2	7.3	7.7	8.8	8.0	9.0	7.9	5.1	9.9
Ray [<i>R</i>]	13.0	17.8	12.8	12.6	12.3	17.6	14.7	12.3	16.6	10.8
Fiber [<i>F</i>]	79.8	76.0	79.9	79.7	78.9	74.4	76.3	79.8	78.3	79.3
Area ratios of the wall in the wood fiber domain (%) measured at high magnification										
G-layer [<i>g</i>]	8.77	16.4	7.88	10.20	0.507	1.61	0	0	0	0
Lignified layer [<i>s</i>]	70.2	60.5	63.2	62.5	69.1	63.8	60.6	62.0	67.9	65.9
Frequency of the fiber cell in the wood fiber domain (/ 0.01 mm ²)										
Total wood fiber	99	107	98	102	85	95	120	84	86	82
G-fiber	51	73	34	44	3	11	0	0	0	0
Relative frequency of G-fiber [ϕ]	0.51	0.68	0.35	0.43	0.04	0.12	0	0	0	0
Physical properties										
Released strain [ϵ_{\parallel}^X] (%)	-0.218	-0.204	-0.094	-0.190	-0.024	-0.038	-0.003	-0.039	0.004	-0.020
Oven-dried shrinkage [α_{\parallel}^X] (%)	1.16	1.10	0.48	0.93	0.24	0.52	0.51	0.50	0.22	0.018
Green Young's modulus [E_{\parallel}^X] (GPa)	10.78	9.21	8.42	11.07	8.92	6.57	7.15	6.37	5.59	7.35
Microfibril angle in the S2 layer (degrees)	Tension wood region					Normal wood region				
Number of the measured fiber	32					32				
Average [θ] (degrees)	23.1					27.2				
Standard deviation (degrees)	(2.18)					(3.38)				

cho, Gifu prefecture, Japan, 14cm in diameter at breast height (DBH), having a leaning stem, was used for the experiment. At breast height, ten measuring points were set peripherally on the xylem surface of the leaning stem. At each point, the released strain of the longitudinal growth stress on the xylem surface (ϵ_{\parallel}^X) was measured using the ordinary strain-gauge method in early April 1988. Thereafter, rectangular portions, $70 \times 10 \times 5$ mm and $50 \times 10 \times 5$ mm in the longitudinal (L), tangential (T), and radial (R) directions, respectively, were sampled away from the upper or lower positions at each measuring point of the released strain. Then, respective portions were used to obtain the tensile Young's modulus under the green condition (E_{\parallel}^X) and the longitudinal shrinkage (α_{\parallel}^X) from green to the oven-dried condition.³

After that, a transverse section, $10\mu\text{m}$ in thickness, was cut from each measuring point of the released strain by a sliding microtome, and the section was stained by safranin and ferric hematoxylin. The section was then mounted on a slide glass with the jelly-like compound of gelatin, glycerin, and water. By using a light microscope connected to an image processor, microscopic images at large and small magnification were photographed within the outermost annual ring of the mounted section. From the images at small magnification, the area composition domain of each tissue, e.g., vessel element (*V*), ray tissue (*R*), and wood fiber (*F*), was computed. From the images at large magnification, the area ratios of the lignified layer (*s*), the G-layer (*g*), and the cell lumen in the domain of the wood fiber were determined. Frequency of the G-fiber per unit area (N_g) in the domain of the wood fiber and that of the normal wood fiber (N-fiber) (N_n) were also counted.

Flat-sliced samples, $5 \times 5 \times 0.015$ mm in L, T, and R respective directions, were cut from the outermost annual rings of both the NW xylem and the highly developed TW xylem. Sampled specimens from the TW xylem were quickly dried with ethanol, and were ultra-sonicated in water to remove the G-layers from the lignified layer.⁷ There-

after, the microfibril angles in the middle layer of the secondary wall (MFA) were measured by the iodine-staining method.⁸

Observed results

Results are summarized in Table 1, which was already reported in our previous report.³ From Table 1, it can be clearly understood that the TW xylem shows quite distinctive properties when compared with the NW xylem. It is considered that either of the G-layer formation or the relatively small MFA in the S2 layer of the G-fiber would cause the distinctive xylem properties in the TW. However, it is still unknown which possibility is more concerned with the origin of the TW properties, or whether there is some other factor that causes the TW properties. In the present article, we attempt to answer this question through simulating the mechanical behaviors of the G-fiber on the basis of the formula derived in our previous report.⁶

Simulation

G-fiber model

A schematic model of the typical G-fiber, consisting of the compound middle lamella (CML), the S1 and S2 layers, and the G-layer, are shown in Fig. 1.⁶

Parameters in the basic formula

In this report, we focus on three biomechanical processes in the TW xylem: (1) cell wall maturation, (2) elastic deformation due to action of an axial traction under a steady moisture condition, and (3) moisture adsorption. The G-fiber tends to shrink or expand in its longitudinal or

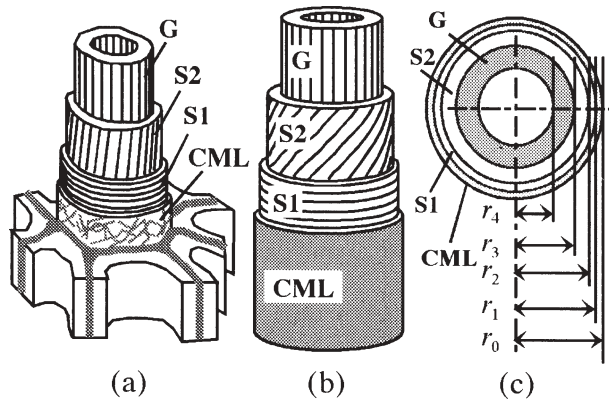


Fig. 1a–c. Multilayered structure of the gelatinous fiber. **a** Microscopic structure, **b** a mechanical model, **c** crosscut surface of the mechanical model. Each consists of compound middle lamella (CML), the outermost layer of the secondary wall (S1), its middle layer (S2), and gelatinous layer (G)

transverse directions when the biomechanical processes occur. We denoted the strains of the dimensional changes of the single G-fiber in the longitudinal and the diametral directions as ε_L and ε_T , respectively, which were simulated by the formula derived in our previous report. Correctly speaking, it is not a model for the behaviors of an isolated fiber, because the constitutive equations used in the formulation consider the conditions of shear restraint imposed by neighboring fibers. A basic formula to calculate ε_L and ε_T contains several parameters, which can be categorized into groups as follows.

Anatomical factors

Anatomical factors are defined as follows:

- r_0, r_1, r_2, r_3 : Outer radii in the CML, the S1 and S2 layers, and the G-layer, respectively.
 r_4 : Innermost radius in the G-fiber.
 $\rho_0, \rho_1, \rho_2, \rho_3$: Ratios of the outer radii to the inner radii in the CML, the S1 and S2 layers, and the G-layer, respectively.
 $\rho_0 = r_0/r_1, \rho_1 = r_1/r_2, \rho_2 = r_2/r_3, \rho_3 = r_3/r_4$.
 h : Thickness of the CML ($= r_0 - r_1$).
 θ : Microfibril angle in the S2 layer (MFA).

Mechanical factors

Mechanical factors are defined as follows:

- E_1, E_2, E_3 : Young's moduli of the framework bundles of the polysaccharide oriented in the direction parallel to the molecular chain of the cellulose in the S1 and S2 layers, and the G-layer, respectively.
 S_1, S_2, S_3 : Double shear moduli of the isotropic skeletons of the matrix substances in the S1 and S2 layers, and the G-layer, respectively.
 S_0 : Double shear modulus of the CML.

Internal expansive terms

Internal expansive terms are defined as follows:

$\varepsilon_1^f, \varepsilon_2^f, \varepsilon_3^f$: Internal strains in the polysaccharide framework bundles in the directions parallel to the cellulose molecular chains in the S1 and S2 layers, and the G-layer, respectively.
 $\varepsilon_1^m, \varepsilon_2^m, \varepsilon_3^m$: Internal strains in the matrix skeletons in the S1 and S2 layers, and the G-layer, respectively. Internal strains are caused by the changes of the physical state in the cell wall.

Basic equations to calculate the dimensional changes of the single G-fiber

The basic equations that give ε_L and ε_T were derived in our previous report.⁶

$$\begin{aligned} \dot{\varepsilon}_L &= f_{11}(\mathbf{p})\dot{\varepsilon}_1^m + f_{12}(\mathbf{p})\dot{\varepsilon}_2^m + f_{13}(\mathbf{p})\dot{\varepsilon}_3^m + f_{14}(\mathbf{p})\dot{\varepsilon}_1^f + f_{15}(\mathbf{p})\dot{\varepsilon}_2^f \\ &\quad + f_{16}(\mathbf{p})\dot{\varepsilon}_3^f + f_{17}(\mathbf{p})\dot{P}_L \\ \dot{\varepsilon}_T (= \dot{\varepsilon}_i|_{r=r_1}) &= f_{21}(\mathbf{p})\dot{\varepsilon}_1^m + f_{22}(\mathbf{p})\dot{\varepsilon}_2^m + f_{23}(\mathbf{p})\dot{\varepsilon}_3^m + f_{24}(\mathbf{p})\dot{\varepsilon}_1^f \\ &\quad + f_{25}(\mathbf{p})\dot{\varepsilon}_2^f + f_{26}(\mathbf{p})\dot{\varepsilon}_3^f + f_{27}(\mathbf{p})\dot{P}_L \end{aligned} \quad (1)$$

where a dot over a character represents the derivative by an elapsed time t . Coefficients $f_{11}, f_{12}, \dots, f_{27}$ are functions of \mathbf{p} , and \mathbf{p} is a parameter vector whose components are $\rho_0, \rho_1, \rho_2, \rho_3, \theta, E_1, E_2, E_3, S_0, S_1, S_2,$ and S_3 . Some parameters depend on t during the cell wall maturation, or the moisture adsorption. P_L represents an axial traction that acts on both ends of the G-fiber. We can calculate the dimensional change of the single wood fiber by integrating the differential Eqs. 1 along the physical state change of the cell wall.

Time-dependent or moisture-dependent behaviors of parameters

Maturation process of the cell wall

The amorphous constituents, such as xylan and lignin, are irreversibly accumulated among the gaps of the polysaccharide bundle after the completion of the polysaccharide framework of the CMF and other oriented polyose. In this process, the amorphous constituent hardens into the matrix skeleton. Thus, $S_1, S_2,$ and S_3 tend to increase monotonously from very small values to their final values. Moreover, the amount of the substance increases irreversibly inside the matrix skeleton whose volume is spatially limited. As the inevitable consequence, internal strains $\varepsilon_1^m, \varepsilon_2^m,$ and ε_3^m are induced in the S1 and S2 layers, and the G-layer, respectively.

It is considered that time-dependent changes in $E_1, E_2,$ and E_3 are somewhat smaller than in $S_1, S_2,$ and S_3 because the polysaccharide framework had been already completed before the matrix substance began to deposit. However, we should not ignore the possibility that aging effects, such as an increase in the crystallinity of the CMF, would generate internal strains $\varepsilon_1^f, \varepsilon_2^f,$ and ε_3^f in the polysaccharide framework bundle.^{3,6,9–11} In such a case, we need to assume a certain value for each of them.

Drying process in the cell wall

Because the completed xylem (i.e., green wood) contains much water, drying is required before converting the wood into natural resources for building or for producing furniture. In this process, the water molecule is discharged from the absorption site in the matrix skeleton, after which the matrix skeleton tends to shrink and harden. This means that S_1 , S_2 , S_3 , ε_1^m , ε_2^m , and ε_3^m tend to change their values monotonously in accordance with the moisture desorption. At the same time, a certain physicochemical change may occur in the bundle of the CMF. However, it is natural to consider that changes of E_1 , E_2 , E_3 and values of ε_1^f , ε_2^f , and ε_3^f are somewhat smaller than those of S_1 , S_2 , S_3 , ε_1^m , ε_2^m , and ε_3^m because the crystal domain, which is a main component of the polysaccharide framework, almost does not participate in the adsorption of the water molecule.

Determination of the values to be assumed for parameters in Eqs. 1

Anatomical factors ρ_0 , ρ_1 , ρ_2 , ρ_3 , and θ

To determine the values of ρ_0 , ρ_1 , ρ_2 , and ρ_3 , it is required to know the ratio of the area of each layer to the total crosscut area of a single wood fiber. Then, we interrelate the parameters ρ_0 , ρ_1 , ρ_2 , and ρ_3 by using the following formuluses (see Appendix A).

$$\begin{aligned} \rho_0 \rho_1 \rho_2 &= \frac{1}{\sqrt{1-s}}, \quad \rho_0 = 1 + \frac{h}{r_1}, \\ \rho_2 &= \frac{1}{\rho_1(1+h/r_1)\sqrt{1-s}}, \quad \rho_3 = \sqrt{\frac{1-s}{(1-s)-f \cdot g/N_g}} \quad (2) \\ & \text{(for } N_g \neq 0), \quad \text{or } \rho_3 = 1 \text{ (for } N_g = 0), \end{aligned}$$

where s and g represent the area ratios of the lignified layer (= CML + S1 + S2) and the G-layer in the domain of the wood fiber, respectively. f and N_g represent the numbers of the wood fiber and the G-fiber per unit area in the domain of the wood fiber. These are experimentally determined values. To determine the values of ρ_0 , ρ_1 , and ρ_2 by using Eqs. 2, we need to give at least two of them. In the present calculation, and with reference to previous studies,^{5,12} we hypothesized 0.025 as the value of h/r_1 , and 1.1 as the value of ρ_1 . Thereafter, for each measuring point of the released strain, we calculated the values of ρ_2 and ρ_3 by using Eqs. 2. The estimated values of ρ_2 and ρ_3 are displayed in Table 2.

θ is one of the anatomical factors in \mathbf{p} . In the present simulation, we used the measured values of the MFA in the S2 layer of the N- and G-fibers, which are displayed in Table 1.

Mechanical factors

The S1 and S2 layers, and the G-layer can be regarded as the parallel composites of the crystalline bundle of cellulose and the matrix skeleton. It follows that the simple mixture law can be applied to calculate the values of E_1 , E_2 , E_3 , S_1 , S_2 , and S_3 as follows:¹²

$$\begin{aligned} E_1 &= A_1 \times C_1 \times E_{\text{cry}}, \quad E_2 = A_2 \times C_2 \times E_{\text{cry}}, \\ E_3 &= A_3 \times C_3 \times E_{\text{cry}}, \\ S_1 &= \frac{(1 - A_1 C_1) E_{\text{matr}}}{1 + \nu}, \quad S_2 = \frac{(1 - A_2 C_2) E_{\text{matr}}}{1 + \nu}, \quad (3) \\ S_3 &= \frac{(1 - A_3 C_3) E_{\text{matr}}}{1 + \nu}, \end{aligned}$$

where ν is Poisson ratio, which is hypothesized to be 0.5 in the same way as in our previous reports.^{6,11-13} C_1 , C_2 , and C_3 are crystallinity indices of the polysaccharide framework in the S1 and S2 layers, and the G-layer, respectively. A_1 , A_2 , and A_3 are weight ratios of the polysaccharide framework in the respective layers. In this study, the values of A_1 , A_2 , and A_3 are assumed as given in Table 3.

E_{matr} is the Young's modulus of the molded matrix substance, which clearly depends on the elapsed time during the cell wall maturation (or moisture content during moisture adsorption). With reference to Cousins's experiments,^{14,15} it is assumed that $E_{\text{matr}} = 2$ GPa in the green condition, and $E_{\text{matr}} = 4-6$ GPa in the dried condition. On the other hand, it is considered that the Young's modulus of the cellulose crystal along the direction parallel to the molecular chain (E_{cry}) is not affected by moisture adsorption. With reference to the study of Nishino et al.,¹⁶ we assume $E_{\text{cry}} = 134$ GPa regardless of the moisture content.

Then we assumed the values and t -dependent patterns of E_1 , E_2 , E_3 , S_1 , S_2 , and S_3 as displayed in Table 3 on the basis of the above-mentioned discussions and the subsidiary conditions described hereafter, provided that the noncrystalline region in the framework bundle was regarded as the matrix substance from the mechanical point of view. The value of S_0 was calculated by the method described in our previous report.¹²

Table 2. Values of the parameters ρ_2 and ρ_3 which are estimated from Eqs. 2

Measuring positions	1	2	3	4	5	6	7	8	9	10	Mean
ρ_2	1.625	1.411	1.462	1.448	1.596	1.474	1.413	1.439	1.558	1.519	1.494 ^a
ρ_3	1.527	1.598	1.616	1.645	1.367	1.274	1.000 ^b	1.000 ^b	1.000 ^b	1.000 ^b	1.505 ^c

^aNo significant difference among the positions (goodness of fit)

^bNo G-fiber was formed at positions 7, 8, 9, and 10

^cMean value for the six positions where G-fiber is formed

Table 3. Values of parameters used for the simulation.**a** Chemical composition in each layer

Layer	Polysaccharide framework (%)	Matrix substance (%)	Crystallinity of the framework
CML	15	85	100 (%)
S1	26	74	C_1
S2	52	48	C_2
G	90	10	C_3

b Time-dependent changes of the mechanical properties of constituents

Time ^a	E_{cry}	$E_{\text{matr}}^{\text{b}}$ (in S1)	$E_{\text{matr}}^{\text{b}}$ (in S2)	$E_{\text{matr}}^{\text{b}}$ (in G)	S_0^{b}
$t = 0 \sim T_1^{\text{c}}$	134	Increase from 0 to 2	0	0	4
$t = T_1 \sim T_2^{\text{c}}$	134	2	Increase from 0 to 2	0	4
$t = T_2 \sim T_3^{\text{c}}$	134	2	2	Increase from 0 to 2	4
$t = T_3 \sim T_4^{\text{d}}$	134	Increase from 2 to 4	Increase from 2 to 4	Increase from 2 to 4	4

c Geometrical properties of the layers

Time ^a	ρ_0	ρ_1	ρ_2	ρ_3^{e}	θ^{fg}
$t = 0 \sim T_1^{\text{c}}$	1.025	1.1	1.494	1.0 or 1.505	27.2 or 23.1
$t = T_1 \sim T_2^{\text{c}}$	1.025	1.1	1.494	1.0 or 1.505	27.2 or 23.1
$t = T_2 \sim T_3^{\text{c}}$	1.025	1.1	1.494	1.0 or 1.505	27.2 or 23.1
$t = T_3 \sim T_4^{\text{d}}$	1.025	1.1	1.494	1.0 or 1.505	27.2 or 23.1

CML, compound middle lamella

^a Assumed with reference to Subsidiary condition 1^b Unit: GPa^c Maturation process after the formation of the polysaccharide framework in the S1, the S2, and the G-layers^d Drying process from the fiber saturation point (FSP) ($t = T_3$), to the oven-dried state ($t = T_4$). $\tau = (T_4 - t)/(T_4 - T_3)$ ^e $\rho_3 = 1.0$ in the N-fiber, $\rho_3 = 1.505$ in the G-fiber^f Unit: degrees^g $\theta = 27.2$ in the N-fiber, $\theta = 23.1$ in the G-fiber**Internal expansive terms**

Neither of the values nor t -dependent patterns can be measured for the internal expansive terms ε_1^{f} , ε_2^{f} , ε_3^{f} , ε_1^{m} , ε_2^{m} , and ε_3^{m} . However, we can optimize their values and t -dependent patterns so as to obtain a reasonable simulation.

Results

Young's modulus of the green G-layer

Experimental results

Matured secondary xylem of kohauchiwakaede consists of four tissue domains, i.e., the wood fiber, the vessel element, the ray parenchyma, and the axial parenchyma. It is considered that these tissues are arranged in a row in the direction parallel to the axis of wood fiber, and the following formula can be used for calculating the longitudinal Young's modulus of the TW xylem (E_{L}^{X}) by the simple law of mixture.

$$E_{\text{L}}^{\text{X}} = \frac{1}{F + V + R + P} (F \cdot E_{\text{L}}^{\text{F}} + V \cdot E_{\text{L}}^{\text{V}} + R \cdot E_{\text{L}}^{\text{R}} + P \cdot E_{\text{L}}^{\text{P}}), \quad (4)$$

where E_{L}^{F} , E_{L}^{V} , E_{L}^{R} , and E_{L}^{P} are Young's moduli of the wood fiber, vessel element, ray parenchyma, and axial parenchyma, respectively, under the green condition, and $F + V + R + P = 1$. Considering $E_{\text{L}}^{\text{V}}/E_{\text{L}}^{\text{F}} \ll 1$, $E_{\text{L}}^{\text{R}}/E_{\text{L}}^{\text{F}} \ll 1$, and $E_{\text{L}}^{\text{P}}/E_{\text{L}}^{\text{F}} \ll 1$, we obtain $E_{\text{L}}^{\text{X}} = E_{\text{L}}^{\text{F}}/F$. In the case of kohauchiwakaede, the amount of the axial parenchyma is somewhat less than that of the other tissues, and its morphological features are similar to the wood fiber cell apart from the fact that the wall thickness of the axial parenchyma is smaller than that of the wood fiber. In this study, for simplification, we did not distinguish the axial parenchyma from the wood fiber when we determined the values of F , V , R , and P .

According to the observations, there was no significant difference among the measuring points on the periphery for the morphological properties of the G-fiber, e.g., the thickness of the lignified layer, that of the G-layer, and their morphological appearances. The same can be said in the

case of the N-fiber. Then, by applying the simple mixture law to the fiber domain that is regarded as a parallel composite of the G-fiber and the N-fiber, we obtain the following formula:

$$E_L^F = \phi \cdot E_L^G + (1 - \phi)E_L^N = (E_L^G - E_L^N)\phi + E_L^N, \quad (5)$$

where $\phi = N_g/f$, $N_g + N_n = f$

E_L^G and E_L^N are the axial Young's modulus of the green G-fiber and that of the green N-fiber, respectively, and ϕ is the relative frequency of the G-fiber in the fiber domain. On the other hand, we obtained the relationship between ϕ and E_L^F ($= E_L^X/F$) as shown in Table 1, which was approximated by the following linear regression:

$$E_L^F = 7.74\phi + 8.50 \quad (r = 0.857). \quad (6)$$

Then, comparing Eqs 5 and 6 directly, we obtain

$$E_L^G = 16.24 \text{ GPa}, \quad E_L^N = 8.50 \text{ GPa}, \quad (7)$$

provided that we do not use the data obtained from measuring point 5 when deriving Eq. 6. This is because the observed value of the longitudinal Young's modulus at measuring point 5 was larger regardless of having very small amount of G-fiber formation, and therefore the estimated value of E_L^G becomes abnormally large at position 5 in comparison with that at the other positions. It is reasonable to assume that some error occurred in measuring the elastic modulus of the specimen at position 5.

Simulation using the wood fiber model

In this simulation, we assumed the condition of the steady moisture state (green condition, i.e., the state at $t = T_3$ in Table 3). Then every component in \mathbf{p} must be constant, and both $d\varepsilon_i^m$ and $d\varepsilon_i^f$ ($i = 1, 2, 3$) should all be nil. Then, from Eqs. 1, we obtain the following formula to calculate the longitudinal Young's modulus of the wood fiber (E_L):

$$E_L = \left\{1/(\pi r_0^2)\right\} dP_L/d\varepsilon_L = \left\{1/(\pi r_0^2)\right\}/f_{17}(\mathbf{p}). \quad (8)$$

The values assumed in Table 3 were used for the simulation using Eq. 8. Firstly, we optimized the values of C_1 and C_2 in Eqs 3 to simulate the experimentally determined value of E_L^N ($= 8.50$ GPa). In this simulation, we assumed that the degree of crystallinity in the framework bundle of the oriented polysaccharide was identical in the S1 and the S2 for convenience, because there is no reason for considering that properties of the CMF are different in the S1 and the S2 layers. Thereafter, we applied the optimized values of C_1 and C_2 to the simulation of E_L in the green G-fiber, and optimized the values of C_3 to obtain the experimentally determined value of E_L^G ($= 16.24$ GPa). Finally, the optimized values of C_1 , C_2 , and C_3 became:

$$C_1(= C_2) = 0.494, \quad C_3 = 0.221. \quad (9)$$

From this result, we calculated the longitudinal Young's modulus of the lignified layer in the N-fiber (E_N^n), that of the lignified layer in the G-fiber (E_N^g), and that of the G-layer (E_G^g) as follows:

$$\text{In the N-fiber: } E_N^n = 13.13 \text{ GPa} \quad (10)$$

$$\text{In the G-fiber: } E_N^g = 16.28 \text{ GPa}, \quad E_G^g = 28.27 \text{ GPa}.$$

Growth strain in the G-layer

Experimental results

The wood fiber, vessel element, ray parenchyma, and axial parenchyma in the differentiating xylem tend to deform during their secondary wall maturation. Thus, the growth strain is generated in the maturing xylem. The infinitesimal increase in the longitudinal growth strain of the xylem at the macroscopic level (ε_L^X) can be expressed by the following formula by the simple mixture law:

$$d\varepsilon_L^X = \frac{F \cdot E_L^F \cdot d\varepsilon_L^F + V \cdot E_L^V \cdot d\varepsilon_L^V + R \cdot E_L^R \cdot d\varepsilon_L^R + P \cdot E_L^P \cdot d\varepsilon_L^P}{F \cdot E_L^F + V \cdot E_L^V + R \cdot E_L^R + P \cdot E_L^P} \quad (11)$$

where $d\varepsilon_L^F$, $d\varepsilon_L^V$, $d\varepsilon_L^R$, and $d\varepsilon_L^P$ are infinitesimal increases of the longitudinal growth strain in the respective tissues. Assuming $E_L^V/E_L^F \ll 1$, $E_L^R/E_L^F \ll 1$, $E_L^P/E_L^F \ll 1$, and $F + V + R + P = 1$, we obtain

$$d\varepsilon_L^X \cong d\varepsilon_L^F.$$

Moreover, we obtain the following formula:

$$\begin{aligned} d\varepsilon_L^X (\cong d\varepsilon_L^F) &= \frac{\phi \cdot E_L^G \cdot d\varepsilon_L^G + (1 - \phi) \cdot E_L^N \cdot d\varepsilon_L^N}{\phi \cdot E_L^G + (1 - \phi) \cdot E_L^N} \\ &= \frac{(E_L^G \cdot d\varepsilon_L^G - E_L^N \cdot d\varepsilon_L^N) \cdot \phi + E_L^N \cdot d\varepsilon_L^N}{(E_L^G - E_L^N) \cdot \phi + E_L^N} \end{aligned} \quad (12)$$

where $d\varepsilon_L^G$ and $d\varepsilon_L^N$ are respective increments in the longitudinal growth strain of the G-fiber and the N-fiber, respectively. By integrating Eq. 12 along the cell wall maturation, we can obtain the growth strain of the newly formed xylem (ε_L^X).

In order to integrate Eq. 12, we also need to know the changes of E_L^G and E_L^N during the process of secondary wall maturation. It is considered that deposition of the matrix constituents has almost no effect on the increases of E_L^G and E_L^N because the stiffness of the matrix substance is somewhat smaller than that of the framework bundle. Therefore, it is natural to consider that increases of E_L^G and E_L^N are caused by a certain qualitative change of the CMF, such as further crystallization of cellulose.¹⁷ Unfortunately, it is still quite difficult to know the time-dependent change of the CMF crystallinity in the cell wall. In the present study, for convenience, we assumed that the crystallinity in each layer is almost unchanged during cell wall maturation. We then hypothesized that the E_L^G and E_L^N become constant through the cell wall maturation.

Growth-stress generation is a biomechanical process during maturation (lignification) of the secondary wall.^{11,17,18} Thus, we integrate Eq. 12 along the cell wall maturation in the G-fiber. As the result, we obtain the following formula:

$$\begin{aligned}\varepsilon_L^x (\cong \varepsilon_L^F) &= \frac{\phi \cdot E_L^g \cdot \varepsilon_L^g + (1 - \phi) \cdot E_L^n \cdot \varepsilon_L^n}{\phi \cdot E_L^g + (1 - \phi) \cdot E_L^n} \\ &= \frac{(E_L^g \cdot \varepsilon_L^g - E_L^n \cdot \varepsilon_L^n) \cdot \phi + E_L^n \cdot \varepsilon_L^n}{(E_L^g - E_L^n) \cdot \phi + E_L^n}\end{aligned}\quad (13)$$

where

$$\varepsilon_L^g = \int_{\text{Maturation process}} d\varepsilon_L^g, \quad \varepsilon_L^n = \int_{\text{Maturation process}} d\varepsilon_L^n.$$

Results from Eq. 7 were used as the values of E_L^g and E_L^n in this formula. The observed relationship between ϕ and ε_L^x ($= \varepsilon_L^F$), which is shown in Table 1, was approximated by the following curvilinear regression:

$$\varepsilon_L^F = -0.5554 + \frac{0.6003}{\phi + 1.098} \cdot (r = 0.956) \quad (14)$$

By comparing Eqs. 13 and 14 directly, we obtained the growth strains of G-fiber (ε_L^g) and the N-fiber (ε_L^n) as follows:

$$\varepsilon_L^g = -0.2693\%, \quad \varepsilon_L^n = -0.0087\%. \quad (15)$$

Simulation based on the G-fiber model

We integrated the basic formula of Eq. 1 during the G-fiber wall maturation under the assumption of $dP_L = 0$. As initial conditions, we adopted $\varepsilon_L(t)|_{t=0} = 0$, $\varepsilon_T(t)|_{t=0} = 0$. Results from Eq. 9 were used as the values of C_1 , C_2 , and C_3 . Values of the parameters assumed in Table 3 were also used for the calculation. We then optimized the increments and t -dependent patterns of ε_1^f , ε_2^f , ε_3^f , ε_1^m , ε_2^m , and ε_3^m to obtain the results in Eq. 15. However, before integrating Eqs. 1, we need to know how the maturation of the G-fiber wall proceeds.

Some scientists clarified the lignification process in the secondary wall of the softwood tracheid and the hardwood normal fiber.^{19,20} On the other hand, maturation of the G-fiber has remained unclear. Recently, based on the technique of immuno-TEM observation, Kim et al.²¹ discovered that the activity of the peroxidase is localized in the secondary wall after the completion of the G-layer. This suggests that lignification proceeds in the secondary wall after the formation of the thick G-layer. With reference to those investigations, we assumed the following conditions regarding the maturation of the G-fiber.

Subsidiary condition 1: Lignification in the S1 layer starts at $t = 0$ after the formation of the frameworks of the cellulose and the other oriented polysaccharide in the secondary wall and the G-layer, and ends at $t = T_1$. This is the first integration interval. Lignification in the S2 layer starts at $t = T_1$, and ends at $t = T_2$. This is the second integration interval. In the G-layer, deposition of a certain matrix substance should proceed, however, no lignification occurs. In this study, as the third integration interval, the deposition of the matrix substance in the G-layer starts at $t = T_2$ and ends at $t = T_3$. Then the G-fiber maturation is completed at $t = T_3$. S_1 , S_2 , and S_3 tend to

increase monotonously and smoothly from very small values to their final values in their respective integration intervals.

We integrate Eqs. 1 as follows:

$$\begin{aligned}\varepsilon_L &= \int_{t=0}^{t=T_3} \left(\frac{d\varepsilon_L}{dt} \right) dt = \int_{\text{The first integration interval}} \left(\frac{d\varepsilon_L}{dt} \right) dt \\ &+ \int_{\text{The second integration interval}} \left(\frac{d\varepsilon_L}{dt} \right) dt + \int_{\text{The third integration interval}} \left(\frac{d\varepsilon_L}{dt} \right) dt\end{aligned}\quad (1')$$

We need to impose certain subsidiary conditions on values and t -dependent patterns of ε_1^f , ε_2^f , ε_3^f , ε_1^m , ε_2^m , and ε_3^m to simulate the observed values of ε_L^n and ε_L^g . In the case of softwood xylem, the observed relationship between the longitudinal growth strain and the MFA in the latewood tracheid can be simulated by supposing [increment in ε_1^m] = 1%, [increment in ε_2^m] = 0.5%, and [increment in ε_1^f] = [increment in ε_2^f] = -0.15%.¹¹ With reference to this result, we assumed the following subsidiary conditions.

Subsidiary condition 2: ε_1^m and ε_2^m take positive values. Each of them increases monotonously and smoothly from 0 to a certain value (= increment) as lignification proceeds in each integration interval.¹¹ It is natural to consider that increments in ε_1^m and ε_2^m depend on the lignin content in the respective layers. This is based on the lignin swelling hypothesis. However, we assume $\varepsilon_3^m = 0$, since no lignification occurs in the G-layer. On the other hand, ε_1^f and ε_2^f take negative values. Each of them tends to change monotonously and smoothly from 0 to a certain value (= increment) with the maturation in each integration interval. This postulates the cellulose tension hypothesis, which considers that the CMF framework tends to contract in the direction parallel to the cellulose molecular chain with the aging of the CMF.^{17,22}

Firstly, we simulated the generation of the growth strain of the N-fiber ($\varepsilon_L^n = -0.0087\%$) by integrating Eq. 1' under the above subsidiary conditions, and optimized the increments in ε_1^f and ε_2^f to obtain the observed value of ε_L^n ($= -0.0087\%$). Thereafter, we tried to simulate the generation of the growth strain of the G-fiber ($\varepsilon_L^g = -0.2693\%$) and optimized the increment ε_3^f . In this simulation, we assumed the following subsidiary condition in addition to the above two conditions:

Subsidiary condition 3: According to the observations by using a light microscope or an ultraviolet microscope, there is no specific difference in the morphological appearance between the secondary wall of the N-fiber and that of the G-fiber.²³ From this fact, we assumed that t -dependent patterns and increments in each of ε_1^m , ε_2^m , ε_1^f , and ε_2^f take identical values between the N-fiber and in the G-fiber.

S_1 , ε_1^f , and ε_1^m are all expressed as monotonously increasing (or decreasing) functions of t in the first integration interval. S_2 , ε_2^f , and ε_2^m are also monotonously increasing (or

Table 4. Combination on the increments in $\varepsilon_1^m, \varepsilon_2^m, \varepsilon_1^f, \varepsilon_2^f$ which optimize the observed value of ε_L^n

ε_1^m (at $t = T_1$) ^a	1	0.8	0.6	0.4	0.2	0	-0.2	-0.4
ε_2^m (at $t = T_2$) ^a	0.5	0.4	0.3	0.2	0.1	0	-0.1	-0.2
ε_1^f (at $t = T_1$) ^b (= ε_2^f at $t = T_2$)	-0.178	-0.145	-0.112	-0.078	-0.045	-0.012	0.021	0.055
ε_T^n (at $t = T_2$) ^c	0.170	0.135	0.099	0.063	0.028	-0.0078	-0.043	-0.079

Data given as percentages

^a Assumed arbitrarily under Subsidiary conditions 1 and 2

^b Calculated from each pair of ε_1^m and ε_2^m to give the observed value of ε_L^n

^c Calculated from each combination of $\varepsilon_1^m, \varepsilon_2^m, \varepsilon_1^f, \varepsilon_2^f$

Table 5. Estimated value of the increment in ε_3^f which gives the observed value of ε_L^n

ε_1^m (at $t = T_1$) ^a	1	0.8	0.6	0.4	0.2	0	-0.2	-0.4
ε_2^m (at $t = T_2$) ^a	0.5	0.4	0.3	0.2	0.1	0	-0.1	-0.2
ε_1^f (at $t = T_1$) ^b (= ε_2^f at $t = T_2$)	-0.178	-0.145	-0.112	-0.078	-0.045	-0.012	0.021	0.055
ε_3^f (at $t = T_3$) ^c	-0.721	-0.737	-0.754	-0.770	-0.786	-0.802	-0.818	-0.834
ε_T^n (at $t = T_3$) ^d	0.333	0.298	0.263	0.228	0.193	0.158	0.123	0.088

Data given as percentages

^a Assumed arbitrarily under Subsidiary conditions 1, 2, and 3

^b Calculated for each pair of ε_1^m and ε_2^m so as to obtain the observed value of ε_L^n

^c Calculated for each combination of $\varepsilon_1^m, \varepsilon_2^m, \varepsilon_1^f, \varepsilon_2^f$ so as to obtain the observed value of ε_L^n

^d Calculated for each combination of $\varepsilon_1^m, \varepsilon_2^m, \varepsilon_1^f, \varepsilon_2^f$, and ε_3^f

decreasing) functions of t in the second integration interval. The same can be said for S_3, ε_3^f , and ε_3^m in the third integration interval. Each of these monotonously increasing (or decreasing) functions can be transformed into functions that do not contain explicitly T_1, T_2 , and T_3 by transforming the integral variable t into γ ($= t/T_1; 0 < t < T_1$), or ξ ($= (t - T_1)/(T_2 - T_1); T_1 < t < T_2$), or κ ($= (t - T_2)/(T_3 - T_2); T_2 < t < T_3$). Moreover, we know these variable transformations alter corresponding integration intervals in Eq. 1' into an identical one that is from 0 to 1. Thus, the concrete value of Eq. 1' does not depend on T_1, T_2 , and T_3 . Furthermore, we should note that integration of Eq. 1' is not affected by the functional shapes of t -dependent variables if each variable changes its value very smoothly in each integration interval. This is quite reasonable because we consider that the t -dependent changes of these variables gradually proceed with the maturation of the matrix skeleton in the respective layers (see Appendix B).

Thus, we can optimize the value of the increment in ε_3^f as displayed in Table 5 which became quite larger than those in ε_1^f and ε_2^f as shown in Table 4.

Drying shrinkage of the G-layer

Experimental results

We can describe the shrinking process of wood as a function of the moisture content τ that is normalized by the moisture content at the fiber saturation point (FSP). We denote the longitudinal shrinking process of the wood as $\alpha_L^X(\tau)$. According to the definition, the longitudinal shrinkage $\alpha_L^X(\tau)$ must satisfy the following boundary condition, $\alpha_L^X(\tau)|_{\tau=1} = 0$. $\alpha_L^X(\tau)|_{\tau=0}$ ($= \alpha_L^X$) means the oven-dried shrinkage of the wood. An infinitesimal increase of the moisture content ($d\tau$) causes an infinitesimal change in the shrinkage of the wood ($d\alpha_L^X$), which is described in the following formula:

$$d\alpha_L^X = \frac{F \cdot \bar{E}_L^F \cdot d\alpha_L^F + V \cdot \bar{E}_L^V \cdot d\alpha_L^V + R \cdot \bar{E}_L^R \cdot d\alpha_L^R + P \cdot \bar{E}_L^P \cdot d\alpha_L^P}{F \cdot \bar{E}_L^F + V \cdot \bar{E}_L^V + R \cdot \bar{E}_L^R + P \cdot \bar{E}_L^P}, \quad (16)$$

where $d\alpha_L^F, d\alpha_L^V, d\alpha_L^R$, and $d\alpha_L^P$ stand for infinitesimal changes of the longitudinal shrinkage in the respective tissues. $\bar{E}_L^F, \bar{E}_L^V, \bar{E}_L^R$ and \bar{E}_L^P are the respective Young's moduli at the moisture content t . Assuming $\bar{E}_L^V/\bar{E}_L^F \ll 1$, $\bar{E}_L^R/\bar{E}_L^F \ll 1$, $\bar{E}_L^P/\bar{E}_L^F \ll 1$, and $F + V + R + P = 1$, we obtain

$$d\alpha_L^X \cong d\alpha_L^F.$$

We apply the simple mixture law to the fiber domain consisting of the N-fiber and G-fiber in parallel, then, we obtain the following formula:

$$\begin{aligned} d\alpha_L^F (\cong d\alpha_L^X) &= \frac{\phi \cdot \bar{E}_L^g \cdot d\alpha_L^g + (1 - \phi) \cdot \bar{E}_L^n \cdot d\alpha_L^n}{\phi \cdot \bar{E}_L^g + (1 - \phi) \cdot \bar{E}_L^n} \\ &= \frac{(\bar{E}_L^g \cdot d\alpha_L^g - \bar{E}_L^n \cdot d\alpha_L^n) \cdot \phi + \bar{E}_L^n \cdot d\alpha_L^n}{(\bar{E}_L^g - \bar{E}_L^n) \cdot \phi + \bar{E}_L^n}, \end{aligned} \quad (17)$$

where $d\alpha_L^g$ and $d\alpha_L^n$ are infinitesimal changes in the shrinkage of the G-fiber and that of the N-fiber, respectively, and \bar{E}_L^g and \bar{E}_L^n are the axial Young's moduli of the G-fiber and N-fiber, respectively.

We obtain an oven-dried shrinkage of the wood fiber domain $\alpha_L^F (= \alpha_L^X(\tau)|_{\tau=0})$ by integrating Eq. 17 from an arbitrary τ to FSP ($\tau = 1$) and extrapolating $\tau \rightarrow 0$, provided that we need to know the τ -dependent patterns of \bar{E}_L^g and \bar{E}_L^n in advance. Then, we tentatively expressed \bar{E}_L^g and \bar{E}_L^n as follows:

$$\bar{E}_L^g = E_L^g \cdot \xi(\tau), \quad \bar{E}_L^n = E_L^n \cdot \zeta(\tau) \quad (18)$$

where $\xi(\tau)$ and $\zeta(\tau)$ are monotonously decreasing functions for τ , and they satisfy $\xi(\tau)|_{\tau=1} = 1$, and $\zeta(\tau)|_{\tau=1} = 1$. E_L^g and E_L^n are constants, which stand for the axial Young's moduli

Table 6. Combinations of the increments of ε_1^m , ε_2^m , ε_1^f , ε_2^f which optimize the observed value of α_L^n

$\varepsilon_1^m (= \varepsilon_2^m)$ at $t = T_4^{a,b}$	15	12	9	6	3	0	-3	-6
$\varepsilon_1^f (= \varepsilon_2^f)$ at $t = T_4^{b,c}$	-3.345	-2.605	-1.865	-1.126	-0.386	0.353	1.094	1.833
$\alpha_L^{n,d,e}$	9.017	7.361	5.643	3.861	2.010	0.086	-1.915	-3.997

Data given as percentages

^a Assumed arbitrarily

^b Positive sign means that each cell wall constituent swells during water sorption

^c Calculated from each pair of ε_1^m and ε_2^m so as to optimize the observed value of α_L^n

^d Calculated from each combination of ε_1^m , ε_2^m , ε_1^f , ε_2^f

^e Positive sign means that the wood fiber shrinks in diameter from the FSP to the oven-dried state

Table 7. Estimated value of the increments in ε_3^f which gives the observed value of α_L^g

$\varepsilon_1^m (= \varepsilon_2^m = \varepsilon_3^m)$ at $t = T_4^{a,b}$	15	12	9	6	3	0	-3	-6
$\varepsilon_1^f (= \varepsilon_2^f)$ at $t = T_4^{b,c}$	-3.345	-2.605	-1.865	-1.126	-0.386	0.353	1.094	1.833
ε_3^f (at $t = T_4$) ^{b,d}	5.078	4.782	4.486	4.190	3.897	3.603	3.304	3.010
$\alpha_L^{g,e,f}$	13.66	11.14	8.461	5.616	2.588	-0.641	-4.089	-7.784

Data given as percentages

^a Assumed arbitrarily

^b Positive sign means that each cell wall constituent swells during water sorption

^c Calculated from each pair of ε_1^m and ε_2^m so as to optimize the observed value of α_L^n

^d Calculated from each combination of ε_1^m , ε_2^m , ε_3^m , ε_1^f , ε_2^f so as to obtain the observed value of α_L^g

^e Calculated from each combination of ε_1^m , ε_2^m , ε_3^m , ε_1^f , ε_2^f , and ε_3^f

^f Positive sign means that the wood fiber shrinks in diameter from the FSP to the oven-dried state

of the green N-fiber and the green G-fiber, respectively. For simplification, we assumed $\xi(\tau) = \zeta(\tau)$ for all τ , which means the decreasing pattern of the longitudinal Young's modulus in the G-fiber is similar to that in the N-fiber. Then, Eq. 15 becomes

$$d\alpha_L^F (\cong d\alpha_L^X) = \frac{(E_L^g \cdot d\alpha_L^g - E_L^n \cdot d\alpha_L^n) \cdot \phi + E_L^n \cdot d\alpha_L^n}{(E_L^g - E_L^n) \cdot \phi + E_L^n}. \quad (19)$$

Under these assumptions, we substituted the results from Eq. 7 to E_L^g and E_L^n in Eq. 19. As the initial conditions, $\alpha_L^g(\tau)|_{\tau=1} = \alpha_L^n(\tau)|_{\tau=1} = 0$, were required. Thus, Eq. 19 can be integrated over moisture content (from an arbitrary τ to $\tau = 1$). We obtain the oven-dried shrinkage of the wood fiber domain $\alpha_L^F (= \alpha_L^F(\tau)|_{\tau=0})$ as the following formula.

$$\alpha_L^X (\cong \alpha_L^F) = \frac{(E_L^g \cdot \alpha_L^g - E_L^n \cdot \alpha_L^n) \cdot \phi + E_L^n \cdot \alpha_L^n}{(E_L^g - E_L^n) \cdot \phi + E_L^n}. \quad (20)$$

The observed relationship between ϕ and α_L^F , which is shown in Table 1, was approximated by the following curvilinear regression:

$$\alpha_L^F = -2.429 + \frac{2.363}{\phi + 1.098}. \quad (r = 0.867) \quad (21)$$

Then, comparing Eqs. 20 and 21 directly, we obtain the oven-dried shrinkage of the N-fiber (α_L^n) and the G-fiber (α_L^g) as follows:

$$\alpha_L^n = 0.2771\%, \quad \alpha_L^g = 1.3026\%. \quad (22)$$

Simulation based on the G-fiber model

Free dimensional change of the single wood fiber due to moisture adsorption was simulated on the basis of the conditions assumed in Table 3. Thus, dP_L should be null in Eqs.

1. For convenience, we calculated the swelling deformation of the wood fiber model $\varepsilon_L(\tau)$ by integrating Eqs. 1 from $\tau = 0$ to $\tau = 1$. The relationship between swelling $\varepsilon_L (= \varepsilon_L(\tau)|_{\tau=1})$ and oven-dried shrinkage $\alpha_L (= \alpha_L(\tau)|_{\tau=0})$ are related to each other by the following formulas:

$$\alpha_L = \frac{\varepsilon_L}{\varepsilon_L + 1}, \quad \varepsilon_L = \frac{\alpha_L}{1 - \alpha_L}. \quad (23)$$

The integral interval for calculating $\varepsilon_L (= \varepsilon_L(\tau)|_{\tau=1})$ is from the oven-dried state ($t = T_4$; $\tau = 0$) to the FSP ($t = T_3$; $\tau = 1$). It is regarded that the increasing moisture content τ is equivalent to the reciprocal elapsed time t . The results from Eq. 9 were used as the values of C_1 , C_2 , and C_3 in this simulation. Then, we optimized the increments in ε_1^m , ε_2^m , ε_3^m , ε_1^f , ε_2^f , and ε_3^f to obtain the observed values of α_L^n and α_L^g .

Swelling of the softwood tracheid cell wall is mainly caused by swelling of the matrix substance, e.g., hemicellulose, lignin, and noncrystalline cellulose.^{12,24-27} Therefore, it is quite reasonable to postulate that ε_1^m , ε_2^m , and ε_3^m take positive values with the increase of the moisture content, and increase monotonously from 0 to the final values, that is to say, increments.

Firstly, we simulated the swelling of the N-fiber ($\varepsilon_L^n = 0.2779\%$). In doing so, we optimized the values of increments in ε_1^m , ε_2^m , ε_1^f , and ε_2^f to give the observed value of the oven-dried shrinkage $\alpha_L^n (= 0.2771\%)$. In the present simulation, we assumed $\varepsilon_1^m = \varepsilon_2^m = \varepsilon_3^m$, and $\varepsilon_1^f = \varepsilon_2^f$ for convenience.

Optimized values of the increments in ε_1^m , ε_2^m , ε_1^f , and ε_2^f were obtained by the simulation as displayed in Table 6. In our previous report, we succeeded in simulating the observed relationships between the longitudinal and the tangential swellings, and the MFA in the clear wood specimen of sugi (*Cryptomeria japonica*) by supposing that $\varepsilon_1^m =$

$\varepsilon_2^m = 12\%–15\%$, and $\varepsilon_1^f = \varepsilon_2^f = 0\%–1\%$.¹² In the present simulation, optimized ε_1^f and ε_2^f became very small but negative, which means that the polysaccharide framework bundles in the S1 and S2 layers tend to contract in the direction parallel to the cellulose molecular chains in spite of increasing moisture content in the cell wall. It is impossible for the authors to provide any comment on this strange result at this stage. However, their absolute values were very small compared with the increments in ε_1^m and ε_2^m .

We also simulated the oven-dried shrinkage of the G-fiber ($\alpha_L^g = 1.3026\%$), and optimized the value of the increment in ε_3^f . In this simulation, it is assumed that the increment in each of ε_1^m , ε_2^m , ε_1^f , and ε_2^f takes an identical value between the N-fiber and the G-fiber (see Subsidiary condition 3). For convenience, we assume $\varepsilon_1^m = \varepsilon_2^m = \varepsilon_3^m$ in this simulation. Thereafter, we optimized the value of the increment in ε_3^f to obtain the observed value of α_L^g . Results are displayed in Table 7. The optimized value of the increment in ε_3^f became a large positive value which is quite different from those in ε_1^f and ε_2^f .

Discussion

Young's modulus of the green G-layer (E_G^g)

According to the results from Eqs. 7, 9, and 10, the predicted Young's modulus of the green G-layer (E_G^g) became 2.15 times as large as that of the lignified layer in N-fiber (E_N^n), and 1.74 times as large as the one in the G-fiber (E_G^g). In any case, we can say that the longitudinal Young's modulus of the G-layer becomes larger than that of the lignified layer in the G-fiber and N-fiber. The predicted value of the Young's modulus of the lignified layer in the G-fiber (E_G^g) became slightly larger than the one in the N-fiber (E_N^n). This is because we calculated the value of E_N^g in due consideration of an experimental fact that the MFA of the S2 layer in the G-fiber was a little smaller than in the N-fiber. This may be one of the factors to increase the Young's modulus of the TW xylem.

It is well known that the TW becomes very stiffer in the longitudinal direction as it dries. The increase of the Young's modulus of the TW xylem due to drying is highly correlated with the percentage of the G-fiber in the fiber domain.⁴ This suggests that the G-layer becomes abruptly rigid as the water molecule is released. However, the validity of this suggestion remains to be confirmed.

Strangely, the predicted value of the relative crystallinity in the framework bundle of the oriented polysaccharide in the G-layer was somewhat smaller than that in the secondary wall (see results from Eq. 9). According to the formula derived in our previous report,¹² the Young's modulus of the G-layer is highly dependent on the ratio of the cellulosic component. In the present simulation, we assumed it to be 90% in the G-layer, which may be a little larger than the true value in the green G-layer. It is likely that the G-layer contains a substantial amount of noncrystalline polyose, e.g., hemicellulose. As another possibility, we note the fact

that the green G-layer is highly swollen by water, which causes an apparent decrease in the relative crystallinity of the cellulose in the green G-layer. Hitherto, we have referred to the classical data of Norberg and Meier⁷ on the chemical and physical properties of the G-layer in aspen. However, we need to critically verify their conclusion for various species.

Growth strain in the G-layer (ε_3^f)

The simulated value of ε_3^f is more negative than that in the lignified layer (ε_1^f and ε_2^f). This indicates that a large contractive internal strain originates in the polysaccharide framework of the G-layer in the direction of the cellulose molecular chain, which causes a high longitudinal tensile growth stress in the TW xylem.

Shrinkage and swelling of the G-layer due to moisture adsorption

Many authors have considered that the polysaccharide framework does not swell or shrink by the action of moisture adsorption. However, the present simulation shows that the value of ε_3^f , which is the swelling ability of the polysaccharide framework in the G-layer, becomes a large positive value. Conversely, the polysaccharide framework in the G-layer tends to shrink in the direction parallel to the cellulose molecular chain during moisture adsorption. This means that the high longitudinal drying shrinkage in the TW xylem is induced by the drying shrinkage of the G-layer in its axial direction. Recently, Clair and Thibaut²⁸ observed by scanning electron microscopy that the dried G-layer tends to be depressed from the surrounding lignified layer, which supports the predicted results in the present simulation.

References

1. Okuyama T, Yamamoto H, Iguchi M, Yoshida M (1990) Generation process of growth stresses in cell walls. II. Growth stress in tension wood. *Mokuzai Gakkaishi* 36:797–803
2. Okuyama T, Yamamoto H, Yoshida M, Hattori Y, Archer RR (1994) Growth stresses in tension wood. Role of microfibrils and lignification. *Ann For Sci* 51:291–300
3. Yamamoto H, Okuyama T, Sugiyama K, Yoshida M (1992) Generation process of growth stresses in cell walls. IV. Action of the cellulose microfibrils upon the generation of the tensile stresses. *Mokuzai Gakkaishi* 38:107–113
4. Clair B, Ruelle J, Thibaut B (2003) Relationship between growth stress, mechanical–physical properties, and proportion of fibre with gelatinous layer in chestnut (*Castanea sativa* Mill.). *Holzforchung* 57:189–195
5. Yamamoto H, Kojima Y, Okuyama T, Abasolo WP, Gril J (2002) Origin of the biomechanical properties of wood related to the fine structure of the multi-layered cell wall. *J Biomech Eng Trans ASME* 124:432–440
6. Yamamoto H (2004) Role of the gelatinous layer on the origin of the physical properties of the tension wood. *J Wood Sci* 50:197–208
7. Norberg PH, Meier H (1966) Physical and chemical properties of the gelatinous layer in tension wood fibres of aspen (*Populus tremula* L.). *Holzforchung* 6:174–178

8. Saiki H, Xu Y, Fujita M (1989) The fibrillar orientation and microscopic measurement of the fibril angles in young tracheid walls of sugi (*Cryptomeria japonica*) (in Japanese). *Mokuzai Gakkaishi* 3:786–792
9. Yamamoto H, Okuyama T (1988) Analysis of the generation process of growth stresses in cell wall (in Japanese). *Mokuzai Gakkaishi* 34:788–793
10. Yamamoto H, Okuyama T, Yoshida M (1995) Generation process of growth stresses in cell walls. VI. Analysis of the growth stress generation by using cell model having three layers (S1, S2, and I+P). *Mokuzai Gakkaishi* 41:1–8
11. Yamamoto H (1998) Generation mechanism of growth stresses in wood cell walls: roles of lignin deposition and cellulose microfibril during cell wall maturation. *Wood Sci Technol* 32:171–182
12. Yamamoto H, Sassus F, Ninomiya M, Gril J (2001) A model of the anisotropic swelling and shrinking process of wood. Part 2. A simulation of shrinking wood. *Wood Sci Technol* 35:167–181
13. Yamamoto H (1999) A model of the anisotropic swelling and shrinking process of wood. Part 1. Generalization of Barber's wood fiber model. *Wood Sci Technol* 33:311–325.
14. Cousins WJ (1976) Elastic modulus of lignin as related to moisture content. *Wood Sci Technol* 10:9–17
15. Cousins WJ (1978) Young's modulus of hemicellulose as related to moisture content. *Wood Sci Technol* 12:161–167
16. Nishino T, Takano K, Nakamae K (1995) Elastic modulus of the crystalline regions of cellulose polymorphs. *J Polym Sci Part B* 33:1647–1651
17. Wardrop AB (1965) The formation and function of reaction wood. In: Cote WA Jr (ed) *Cellular ultrastructure of woody plants*. Syracuse University Press, New York, pp 373–390
18. Archer RR (1987) Growth stresses and strains in trees. Springer, Berlin Heidelberg New York
19. Terashima N (1990) A new mechanism for formation of a structurally ordered protolignin macromolecule in the cell wall of tree xylem. *J Pulp Paper Sci* 16:J150–J155
20. Donaldson LA (1992) Lignin distribution during latewood formation in *Pinus radiata* D. Don. *IAWA Bull* 13:381–387
21. Kim YS, Wi SG, Grunwald C, Schmitt U (2002) Immuno electron microscopic localization of peroxidases in the differentiating xylem of *Populus* spp. *Holzforschung* 56:355–359
22. Bamber RK (1987) The origin of growth stresses. A rebuttal. *IAWA Bull* 8:80–84
23. Yoshida M, Ohta H, Okuyama T (2002) Tensile growth stress and lignin distribution in the cell walls of black locust (*Robinia pseudoacacia*). *J Wood Sci* 48:99–105
24. Barber NF, Meylan BA (1964) The anisotropic shrinkage of wood. A theoretical model. *Holzforschung* 18:146–156
25. Barrett JD, Schniewind AP, Taylor RL (1972) Theoretical shrinkage model for wood cell walls. *Wood Sci* 4:178–192
26. Cave ID (1972) A theory of shrinkage of wood. *Wood Sci Technol* 2:268–278
27. Koponen S, Toratti T, Kanerva P (1989) Modelling longitudinal elastic and shrinkage properties of wood. *Wood Sci Technol* 23:55–63
28. Clair B, Thibaut B (2001) Shrinkage of the gelatinous layer of poplar and beech tension wood. *IAWA J* 22:121–131

Appendix A Deriving Eqs. 2

We denote the number of the G-fiber in the wood fiber domain with an area A as G and that of the N-fiber as N , provided that $G + N = X$. We set the following assumption.

Assumption A: The thickness of the lignified wall in the G-fiber is identical to that of the N-fiber regardless of the measuring position.

This assumption is not so inappropriate to the wood fiber domain in the real xylem because the observed values of s

and X/A ($= f$) become almost unchanged regardless of measuring positions, as seen in Table 1. Moreover, we set the following assumptions.

Assumption B: The diameter of the G-fiber is similar as that of the N-fiber.

Assumption C: Cellular arrangement in the crosscut surface of the xylem takes a tessellation structure consisting of a polygonal cell.

Then, we can connect the area ratio of the lignified layer [s], and that of the gelatinous layer [g] to ρ_0 , ρ_1 , ρ_2 , and ρ_3 under assumptions A, B, and C.

It may be a little hasty to apply calculated values of ρ_0 , ρ_1 , ρ_2 , and ρ_3 to the simulation using Eqs. 1 because the crosscut shape of the G-fiber model displayed in Fig. 1 is close to circular. However, we know that the hexagon is the most closely allied to the circle in shape among the polygons that constitute the tessellation arrangement. Then, we set the following assumption.

Assumption D: Crosscut shape of the wood fiber in the cellular arrangement is a hexagon with an area of

$$\left(3\sqrt{3}/2\right)r_0^2 \text{ as displayed in Fig. 2.}$$

We denote the thickness of the lignified layer as $(\sqrt{3}/2)(r_0 - r_3)$, and that of the G-layer as $(\sqrt{3}/2)(r_3 - r_4)$. Distances from the central point of the hexagon to the lignified and gelatinous layers are denoted as $(\sqrt{3}/2)r_3$ and $(\sqrt{3}/2)r_4$, respectively. s can be given as in the following formula:

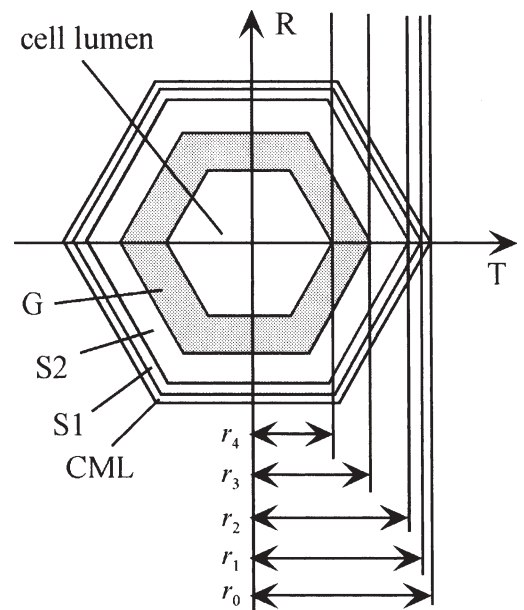


Fig. 2. A hexagon-shaped model of the wood fiber used for calculating Eqs. 2. T , tangential direction; R , radial direction

$$s = \frac{3}{2}\sqrt{3}(r_0^2 - r_3^2)X/A = 1 - \frac{3}{2}\sqrt{3} \cdot r_3^2 \cdot f. \quad (\text{A1})$$

In a similar manner, g is given as the following formula:

$$g = \frac{3}{2}\sqrt{3}(r_3^2 - r_4^2)G/A = (1-s)\frac{G}{X} - \frac{3}{2}\sqrt{3} \cdot r_4^2 \cdot \frac{G}{A}. \quad (\text{A2})$$

X/A , G/A , s , and g can be determined experimentally as displayed in Table 1. From Eqs. A1 and A2, we can obtain r_3 and r_4 as follows:

$$\begin{aligned} r_3 &= \frac{1}{3}\sqrt{2\sqrt{3}(1-s)\frac{A}{X}}, \\ r_4 &= \frac{1}{3}\sqrt{2\sqrt{3}(1-s)\frac{A}{X} - g\frac{A}{G}} \quad (G \neq 0). \end{aligned} \quad (\text{A3})$$

If we denote r_0/r_1 , r_1/r_2 , r_2/r_3 , and r_3/r_4 as ρ_0 , ρ_1 , ρ_2 , and ρ_3 , respectively, we obtain the following equation:

$$\begin{aligned} \rho_0\rho_1\rho_2 &= \frac{1}{\sqrt{1-s}}, \quad \rho_3 = \sqrt{\frac{(1-s)}{(1-s) - g \cdot f/N_g}} \\ &\text{(for } N_g \neq 0\text{), } \rho_3 = 1 \quad \text{(for } N_g = 0\text{),} \end{aligned} \quad (\text{A4})$$

where $f = X/A$, and $N_g = G/A$.

Appendix B Integration (Eq. 1') is not affected by the functional shapes of t -dependent variables $S_1, S_2, S_3, \varepsilon_1^m, \varepsilon_2^m, \varepsilon_3^m, \varepsilon_1^f, \varepsilon_2^f, \varepsilon_3^f$

We introduce functions φ_1 , φ_2 , and φ_3 which vary from 0 to 1 in the range of $0 \leq t \leq T_3$ as follows:

$$\begin{aligned} \varphi_1(t) &= \begin{cases} P(t) & (0 \leq t \leq T_1) \\ 1 & (T_1 \leq t \leq T_3) \end{cases}, \quad \varphi_2(t) = \begin{cases} 0 & (0 \leq t \leq T_1) \\ Q(t) & (T_1 \leq t \leq T_2) \\ 1 & (T_2 \leq t \leq T_3) \end{cases}, \\ \varphi_3(t) &= \begin{cases} 0 & (0 \leq t \leq T_2) \\ R(t) & (T_2 \leq t \leq T_3) \end{cases}, \end{aligned} \quad (\text{B1})$$

where $P(t)$, $Q(t)$, and $R(t)$ are monotonously increasing and differentiable functions, which vary smoothly from 0 to 1 in the respective domains. With reference to Subsidiary conditions 1 and 2, we assume the following condition as the

functional shapes of t -dependent variables $S_i(t)$, $\varepsilon_i^m(t)$, and $\varepsilon_i^f(t)$ ($i = 1, 2, 3$):

$$\begin{aligned} S_i(t) &= k_i \cdot \varphi_i(t), \quad \varepsilon_i^m(t) = m_i \cdot \varphi_i(t), \quad \varepsilon_i^f(t) = n_i \cdot \varphi_i(t). \\ &(i = 1, 2, 3) \end{aligned} \quad (\text{B2})$$

where k_i , m_i , and n_i are constants. It is reasonable to assume this condition if these t -dependent variables change the values smoothly during maturation of the matrix skeleton in their respective integration intervals. Then, by substituting Eq. B2 into Eq. 1', we obtain the following expression:

$$\begin{aligned} \varepsilon_L &= \int_0^{T_1} g_1[\varphi_1(t)] \left(\frac{d\varphi_1(t)}{dt} \right) dt \\ &+ \int_{T_1}^{T_2} g_2[\varphi_2(t)] \left(\frac{d\varphi_2(t)}{dt} \right) dt \\ &+ \int_{T_2}^{T_3} g_3[\varphi_3(t)] \left(\frac{d\varphi_3(t)}{dt} \right) dt. \end{aligned} \quad (\text{B3})$$

$$\text{where } \begin{cases} g_1(\varphi_1(t)) = m_1 \cdot f_{11}(\mathbf{p}) \Big|_{S_1=k_1 \cdot \varphi_1(t)} \\ \quad + n_1 f_{14}(\mathbf{p}) \Big|_{S_1=k_1 \cdot \varphi_1(t)} \quad (0 \leq t \leq T_1) \\ g_2(\varphi_2(t)) = m_2 \cdot f_{12}(\mathbf{p}) \Big|_{S_2=k_2 \cdot \varphi_2(t)} \\ \quad + n_2 f_{15}(\mathbf{p}) \Big|_{S_2=k_2 \cdot \varphi_2(t)} \quad (T_1 \leq t \leq T_2) \\ g_3(\varphi_3(t)) = m_3 \cdot f_{13}(\mathbf{p}) \Big|_{S_3=k_3 \cdot \varphi_3(t)} \\ \quad + n_3 f_{16}(\mathbf{p}) \Big|_{S_3=k_3 \cdot \varphi_3(t)} \quad (T_2 \leq t \leq T_3) \end{cases}$$

From Eq. B1, Eq. B3 is modified into the following expression.

$$\begin{aligned} \varepsilon_L &= \int_{t=0}^{t=T_1} g_1[P(t)] dP(t) + \int_{t=T_1}^{t=T_2} g_2[Q(t)] dQ(t) \\ &+ \int_{t=T_2}^{t=T_3} g_3[R(t)] dR(t). \end{aligned} \quad (\text{B4})$$

$P(t)$, $Q(t)$, and $R(t)$ change the values from 0 to 1 monotonously and continuously for elapsed time t in their respective integration intervals. We can rewrite Eq. B4 as the following expression:

$$\varepsilon_L = \int_0^1 g_1(P) dP + \int_0^1 g_2(Q) dQ + \int_0^1 g_3(R) dR. \quad (\text{B5})$$

This result indicates that the integration value in Eq. B5 does not depend on the concrete values of T_1 , T_2 and T_3 . Furthermore, it is not affected by the functional shapes of the t -dependent variables $S_1, S_2, S_3, \varepsilon_1^m, \varepsilon_2^m, \varepsilon_3^m, \varepsilon_1^f, \varepsilon_2^f, \varepsilon_3^f$ if we assume the condition described by Eq. B2.